The EMBO Journal (2009) 28, 1953–1964 | © 2009 European Molecular Biology Organization | All Rights Reserved 0261-4189/09
www.embojournal.org

THE EMBO JOURNAL

How the MccB bacterial ancestor of ubiquitin E1 initiates biosynthesis of the microcin C7 antibiotic

Catherine A Regni[1], Rebecca F Roush[2], Darcie J Miller[1], Amanda Nourse[3], Christopher T Walsh[2] and Brenda A Schulman[1,4,*]

[1]Department of Structural Biology, St Jude Children's Research Hospital, Memphis, TN, USA; [2]Department of Biological Chemistry and Molecular Pharmacology, Harvard Medical School, Boston, MA, USA; [3]Hartwell Center for Bioinformatics and Biotechnology, St Jude Children's Research Hospital, Memphis, TN, USA and [4]Howard Hughes Medical Institute

The 39-kDa *Escherichia coli* enzyme MccB catalyses a remarkable posttranslational modification of the MccA heptapeptide during the biosynthesis of microcin C7 (MccC7), a 'Trojan horse' antibiotic. The approximately 260-residue C-terminal region of MccB is homologous to ubiquitin-like protein (UBL) activating enzyme (E1) adenylation domains. Accordingly, MccB-catalysed C-terminal MccA-acyl-adenylation is reminiscent of the E1-catalysed activation reaction. However, unlike E1 substrates, which are UBLs with a C-terminal di-glycine sequence, MccB's substrate, MccA, is a short peptide with an essential C-terminal Asn. Furthermore, after an intramolecular rearrangement of MccA-acyl-adenylate, MccB catalyses a second, unique reaction, producing a stable phosphoramidate-linked analogue of acyl-adenylated aspartic acid. We report six-crystal structures of MccB in apo, substrate-, intermediate-, and inhibitor-bound forms. Structural and kinetic analyses reveal a novel-peptide clamping mechanism for MccB binding to heptapeptide substrates and a dynamic-active site for catalysing dual adenosine triphosphate-consuming reactions. The results provide insight into how a distinctive member of the E1 superfamily carries out two-step activation for generating the peptidyl-antibiotic MccC7.

The EMBO Journal (2009) **28,** 1953–1964. doi:10.1038/emboj.2009.146; Published online 4 June 2009
Subject Categories: proteins; structural biology
Keywords: antibiotic; MccB; MccC7; microcin; ubiquitin activating enzyme

Introduction

To survive in a competitive milieu, bacteria generate a variety of antimicrobial agents that are toxic to rival species. Many clinically important antibiotics, such as penicillin, actinomycin, and vancomycin, contain peptide scaffolds that are generated by bacterial non-ribosomal peptide synthetases (Mootz *et al*, 2002). Other antibiotics contain ribosomally synthesized peptides, including the low-molecular weight microcins (Nolan and Walsh, 2008). Microcins are posttranslationally modified peptides that inhibit growth of competing Gram-negative bacteria, such as *Escherichia*, *Salmonella*, and *Enterobacter*, at nanomolar concentrations (Duquesne *et al*, 2007). Microcin C7 (MccC7, Figure 1A), a heptapeptide with an *N*-formylated methionine, an aminopropyl moiety, and a C-terminal phosphoramidate linkage to adenosine (Guijarro *et al*, 1995), is produced by *Escherichia coli* to eradicate competitor strains through a 'Trojan horse' mechanism. After import into target cells, the peptide framework of MccC7 is cleaved by non-specific peptidases to release a toxic adenylated-aspartic-acid mimic that targets aspartyl-tRNA synthetase, and thereby inhibits protein synthesis (Metlitskaya *et al*, 2006).

Understanding the biosynthetic pathways of natural products, such as MccC7, allows us to gain insights into enzyme mechanism, provides opportunities for developing new antibiotics, and gives new prospects for protein design aimed at generating novel biologically active compounds. MccC7 is generated by two posttranslational modifications of a precursor ribosomal heptapeptide, MccA, featuring the sequence MRTGNAN. Posttranslational steps in MccC7 biosynthesis involve the conversion of the C-terminal Asn_7 to an Asp amide, in which the nitrogen is linked by a phosphoramidate bond to adenosine monophosphate (AMP), followed by aminopropylation of one of the phosphate oxygens. The migration of the Asn_7 carboxamido nitrogen and the N–P bond-forming step are catalysed in a Mg^{2+}-dependent manner by the enzyme MccB (Figure 1B) (Roush *et al*, 2008). First, in a conventional acyl-adenylation reaction that consumes one adenosine triphosphate (ATP) molecule, MccB catalyses adenylation of the C-terminus of MccA. The resulting MccA-acyl-adenylate then undergoes intramolecular rearrangement, during which AMP is expelled by the carboxamido nitrogen of Asn_7 as a peptidyl-succinimide intermediate is formed. Next, MccB catalyses an unusual adenylation of the succinimide: the succinimidyl nitrogen attacks the α-phosphate of a second ATP molecule. This links the AMP moiety to the peptide terminus through an N–P bond. The succinimide ring is hydrolysed by regiospecific water-mediated opening to yield the peptidyl-acyl-N-P-adenosine group, which is the Trojan horse reagent. Unlike acyl-adenylate complexes, which are hydrolytically labile-mixed acyl-phosphoric anhydrides, the phosphoramidate-linked analogue of aspartic acyl-adenylate (Figure 1B) is hydrolytically stable, allowing persistence throughout the remainder of the MccC7 biosynthetic pathway (aminopropylation, export by the producing cell and import by a sensitive bacterial cell) and ultimate toxic inhibition of aspartyl-tRNA synthetase and protein synthesis in competing bacteria.

*Corresponding author. Department of Structural Biology, St Jude Children's Research Hospital, MS #311, Room D5024E, 262 Danny Thomas Place, Memphis TN 38105, USA.
Tel.: +1 901 595 5147; Fax: +1 901 595 5785;
E-mail: Brenda.schulman@stjude.org

Received: 17 December 2008; accepted: 8 May 2009; published online: 4 June 2009

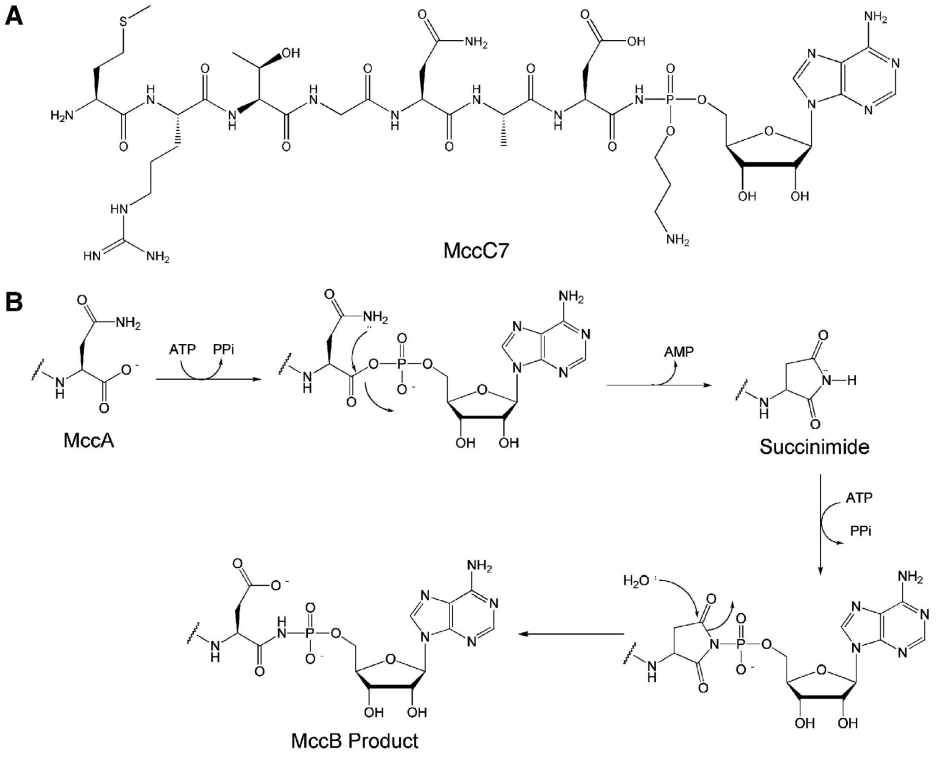

C

Structure	Relevance
Apo	Free enzyme
MccB(MccA)	First peptide substrate
MccB(MgATP)	Nucleotide substrate
MccB(MccA–AMPCPP)	First peptide substrate plus nucleotide non-hydrolyzable analogue
MccB(Succinimide)	Second peptide substrate
MccB(MccA–N7isoAsn)	Inhibitor

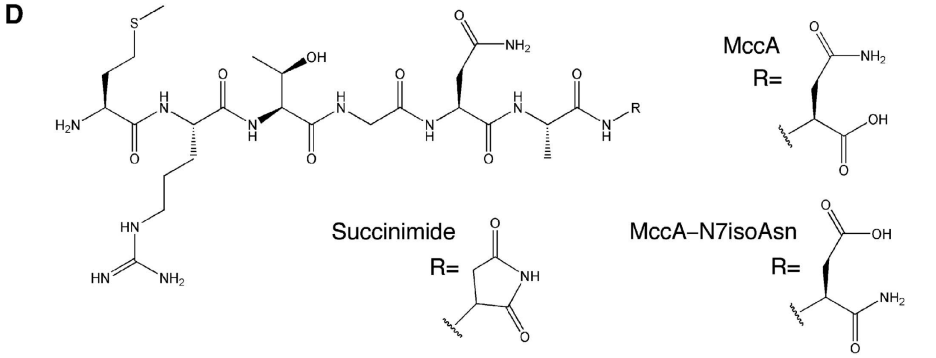

Figure 1 The MccB reaction. (**A**) Structure of MccC7. (**B**) Mechanism for the MccB reaction. Only the C-terminus of the MccA heptapeptide is shown for clarity. (**C**) List of MccB structures presented. (**D**) Chemical structures of the peptides used in this study.

The 351-residue MccB has two discernible regions of sequence. The N-terminal (~90 residues) region is not detectably homologous to known structures. The C-terminal (~260 residues) region shares homology with the adenylation domain portion of ubiquitin-like (UBL) protein-activating enzymes, also called E1s, which initiate UBL conjugation (Supplementary Figures 1 and 2). MccB-catalysed adenylation of the MccA C-terminus is reminiscent of the first E1-catalysed reaction, which is the C-terminal adenylation of UBL substrates. However, the substrates of MccB and E1s

are markedly divergent. Although MccB catalyses C-terminal transformation of a peptide destined for secretion to combat other organisms, substrates of E1s are proteins that serve as sulphur carriers during biosynthetic pathways, or as covalent protein modifiers (Hochstrasser, 2000, 2009).

The sequence similarity between MccB and UBL-activating enzymes raises several questions about common and divergent aspects of the MccB mechanism. First, how does MccB recognize a short-peptide substrate, when all other family members have a $\geqslant$8 kDa UBL protein substrate? Second, why does MccB catalyse adenylation of a peptide harbouring a C-terminal Asn or succinimide, rather than the Gly-Gly sequence found at the C-termini of UBLs? Third, how can MccB catalyse two successive adenylation reactions? To address these questions, we performed structural, biophysical, and biochemical analyses of MccB–MccA–nucleotide interactions.

Results and discussion

Overall structure of MccB

We determined crystal structures of MccB separately and in complex with the following ligands: (1) MccA (first-peptide substrate), (2) MgATP (nucleotide substrate and divalent metal required for catalysis), (3) MccA and α,β-methylene ATP (AMPCPP) (first-peptide substrate and non-hydrolysable ATP analogue), (4) MccA–succinimide (second-peptide substrate), and (5) MccA–N7isoAsn (inhibitor) (Roush *et al*, 2008) (Figure 1C and D; Table I; Supplementary Figure 3). All asymmetric units contain two nearly identical MccB homodimers, with chains designated as A–B or C–D. Thus, the six structures presented here contain a total of 12 homodimers and 24 protomers. The 12 A–B and C–D homodimers superimpose with a Cα root mean square deviation (RMSD) of 76 Å. Owing to this structural similarity, our discussion focuses on chains A–B. The MccB homodimer has an elongated shape. Each homodimer has two parallel, two-domain 'active units'. Each 'active unit' contains an adenylation domain and a globular domain not found in other E1 enzymes. These domains are generated from parts of both protomers in the homodimer (Figure 2).

For the adenylation domain, the two parallel halves comprise residues (1) A104-A260, A287-A351, B90-B103 and (2) B104-B260, B287-B351, A90-A103. Each half includes a Rossmann-fold ATP-binding cleft. A five-stranded β-sheet,

Table I Data collection and refinement statistics

Structure	Apo			MgATP	MccA-N7isoAsn	Succinimide	MccA	MccA-AMPCPP
Space group	$P2_12_12_1$			$P2_1$	$P2_1$	$P2_1$	$P2_1$	$P2_1$
Data collection	Native	Inflection	Remote					
λ (Å)	1.28290	1.28330	1.25000	0.97926	0.97926	1.00000	0.97926	0.97926
Unit cell	$a=144.7$	$a=144.5$	$a=144.8$	$a=55.9$	$a=55.9$	$a=55.9$	$a=56.3$	$a=55.8$
	$b=145.0$	$b=144.7$	$b=144.9$	$b=138.2$	$b=138.2$	$b=138.0$	$b=138.6$	$b=138.0$
	$c=158.7$	$c=158.1$	$c=158.9$	$c=80.2$	$c=80.8$	$c=80.1$	$c=81.4$	$c=80.8$
	$\alpha,\beta,\gamma=90$	$\alpha,\beta,\gamma=90$	$\alpha,\beta,\gamma=90$	$\alpha,\gamma=90$, $\beta=92.6$	$\alpha,\gamma=90$, $\beta=92.4$	$\alpha,\gamma=90$, $\beta=92.1$	$\alpha,\gamma=90$, $\beta=92.1$	$\alpha,\gamma=90$, $\beta=92.2$
Resolution	50–2.8	50–2.8	50–2.9	50–1.85	50–2.2	50–2.1	20–2.63	50–2.3
R_{sym}[a] (%)	10.1 (37.8)	8.6 (37.1)	10.9 (59.3)	5.4 (36.4)	6.5 (37.1)	9.0 (54.6)	8.3 (31.1)	8.1 (36.4)
Completeness %	100 (99.8)	100(100)	100 (99.9)	92.9 (89.0)	96.7 (90.5)	99.9 (99.9)	100 (99.9)	98.9 (91.1)
Redundancy	7.0 (6.5)	7.2 (7.1)	7.2 (7.1)	3.1 (2.8)	4.1 (3.6)	4.4 (4.2)	7.0 (6.4)	4.1 (3.3)
Average $I/\sigma I$	27.2 (4.5)	27.2 (4.6)	21.8 (2.6)	19.2 (2.7)	21.9 (3.0)	22.2 (2.2)	23.3 (4.5)	17.1 (2.1)
Refinement								
Resolution	49.7–2.8			42.6–1.9	46.9–2.2	27.4–2.1	20–2.6	39.9–2.3
Reflections	77 699			84 354	57 050	67 014	36 931	51 038
R_{work}[b] (%)	22.3			20.4	20.3	19.4	20.7	19.6
R_{free}[c] (%)	25.7			25.6	26.1	25.0	27.3	25.5
Total atoms in refinement	11 064			11 310	11 321	10 714	10 571	10 853
Number of atoms								
Protein	11 049			10 425	10 577	10 319	10 298	10 412
Solvent	0			748	511	263	141	223
Peptide	0			—	194	118	118	76
Nucleotide	0			124	0	0	0	133
Zn^{2+}, Mg^{2+}, SO_4^{2-}	4, 0, 0			4, 4, 1	4, 0, 7	4, 0, 2	4, 0, 2	4, 0, 1
Other	11			—	—	—	—	—
RMSD bond (Å)	0.013			0.010	0.009	0.014	0.008	0.010
RMSD angle (°)	1.520			1.306	1.103	1.518	1.369	1.248
Average B (Å^2)	53.2			22.9	36.3	45.1	52.0	44.2
Average B (Å^2)								
Protein	53.9			22.5	36.0	44.8	51.5	43.7
Peptide	—			—	47.8	75.9	106.9	88.2
Nucleotide	—			24.9	—	—	—	74.3
Solvent	—			27.8	37.0	44.0	42.8	37.1
Zn^{2+}, Mg^{2+}, SO_4^{2-}	—, —, —			27.7, 32.4, 46.1	44.6, —, 67.3	51.2, —, 73.9	80.8, —, 96.7	56.3, —, 95.8
Other	59.4			—	—	—	—	—

[a]$\sum|I-\langle I\rangle|/\sum I$, where I, observed intensity; $\langle I\rangle$, average intensity obtained from multiple observations of symmetry-related reflections.
[b]$R_{work}=\sum(\|F_p(obs)-F_p(calc)\|)/\sum|F_p(obs)|$.
[c]$R_{free}=R$ factor for a selected subset (5%) of the reflections that was not included before refinement calculations.

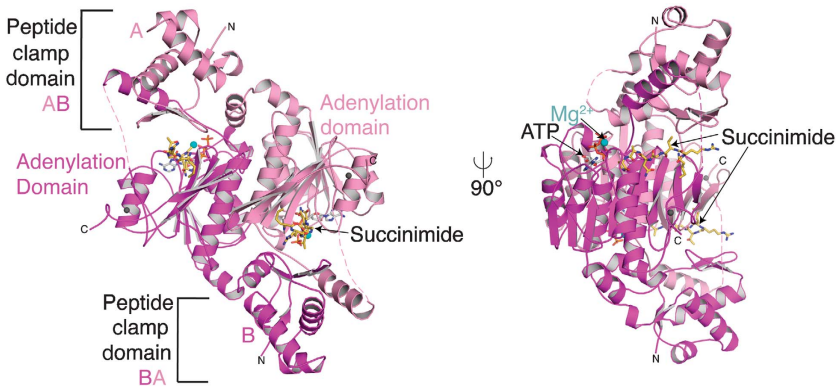

Figure 2 Overall structure of MccB. The MccB–succinimide complex structure is shown, with MgATP modelled into the adenlyation-active site after superposition of MccB–succinimide and MccB–MgATP structures. The two protomers in the MccB homodimer are shown in cartoon representation in pink (chain A) and magenta (chain B), with their amino- and carboxyl-termini labelled N and C, respectively. Dashed lines represent connections between sequences that are not visible in the electron density. The MccB peptide clamp and adenylation domains are indicated with labels coloured to indicate chain A (pink) or B (magenta). MccA–succinimide (succinimide) and ATP are depicted as sticks, with their carbon atoms in yellow and grey, respectively. Nitrogen atoms are shown in blue, oxygen atoms in red, and phosphorous atoms in orange. Mg^{2+} and Zn^{2+} ions are depicted as cyan and grey spheres, respectively.

stabilized by an adjacent zinc-binding site, forms a concave peptide-binding surface. Both halves, individually and together, superimpose with the homologous regions of the bacterial UBL-activating enzymes MoeB and ThiF with Cα RMSDs of 1.5 Å over half and 1.7 Å over the dimer (Lake *et al*, 2001; Duda *et al*, 2005), and with the eukaryotic E1s UBA1, NAE1-UBA3, and SAE1-UBA2 with Cα RMSDs of 1.8–1.9 Å over half and 2.1 Å over the dimer (Walden *et al*, 2003b; Lois and Lima, 2005; Lee and Schindelin, 2008).

The unique MccB domain is formed by the coupling of two separated regions of the MccB sequence: the N-terminal residues 1–87 from one monomer and residues 261–287 from the opposite protomer within the homodimeric assembly (Supplementary Figure 1). This latter region corresponds to an E1 enzyme 'crossover loop', which crosses over the C-terminal tail from the associated UBL (Lake *et al*, 2001; Walden *et al*, 2003a; Lois and Lima, 2005; Lee and Schindelin, 2008). In MccB, the 'crossover loop' is incorporated into the MccB-specific domain, which adopts a structure loosely related to a winged-helix fold. In our peptide co-crystal structures, numerous contacts are observed between this domain and the associated peptides. Thus, we refer to this domain as the 'peptide clamp', owing to its interactions with MccA.

The adenylation and peptide clamp domains pack together in a manner resembling a clamshell. In the overall assembly of an 'active unit', each domain would represent half the shell, which together generate a large central groove that cradles the ATP and peptide substrates (Figure 2).

Anchoring MccA through the unique peptide clamp

Detailed insights into heptapeptide recognition come from superimposing the MccB–MccA and MccB–succinimide structures. MccA extends over MccB's adenylation domain β-sheet with its C-terminus approaching the ATP-binding site for adenylation (Figure 3A). The peptides bind in a groove formed by the adenylation domain β-sheet cleft on one side, and the peptide clamp on the other, burying an average of 940 A^2 from MccA (85% of the total surface area) and ~ 600 A^2 from MccB.

To test the functional importance of the peptide clamp domain, we performed enzymatic assays on mutant versions of MccB. Deleting the MccB N-terminal extension (ΔNTE), which comprises the bulk of the peptide clamp domain, completely eliminates the activity (Figure 3B; Supplementary Figure 4). To test whether a ΔNTE mutant has an intact adenylation domain assembly, we assayed homodimerization by analytical ultracentrifugation (AUC). As the AUC data indicate dimerization, reflecting proper folding (Supplementary Figure 5), we tested whether adding a 10-kDa protein fragment corresponding to MccB's N-terminal 87 residues (NTE) could restore any activity to the ΔNTE mutant in trans. Approximately 20% of the wild-type (WT) activity was restored (Figure 3B; Table II). These results support the importance of the peptide clamp domain, and indicate that the adenylation and peptide clamp domains work together optimally when expressed as a single unit.

Certain MccB residues from both the clamp and adenylation domains contact the peptides in all the co-crystal structures (Figure 4). Two such residues from the clamp domain are K10 and E26. MccB's K10 directly contacts the carbonyl oxygen from G_4 and the T_3 side chain from MccA and the succinimide. This latter interaction may have a function in constraining the sequences allowed at MccA position 3 during MccC7 biosynthesis (Kazakov *et al*, 2007). The MccB–K10A mutant has little effect on catalytic rate, but has an increase in the K_m of MccA (Table II), which further shows its importance for peptide binding.

Residues in the adenylation domain form a pocket, in which the N-terminus of the peptides binds. The peptide N-terminal Met_1 adopts a similar conformation in all the complexes, and is encircled by a deep hydrophobic channel generated by residues I243, V245, W326, and H333. The carbonyl of the peptide Met_1 participates in a hydrogen bonding network with R322 and Q335 (Figure 4). In the absence of peptide (as in the ATP-bound structure), R322 and Q335 are bound to the solvent.

Past Met_1, the next four peptide residues follow related trajectories towards the adenylation-active site. Although none of these structurally represents a catalytic intermediate,

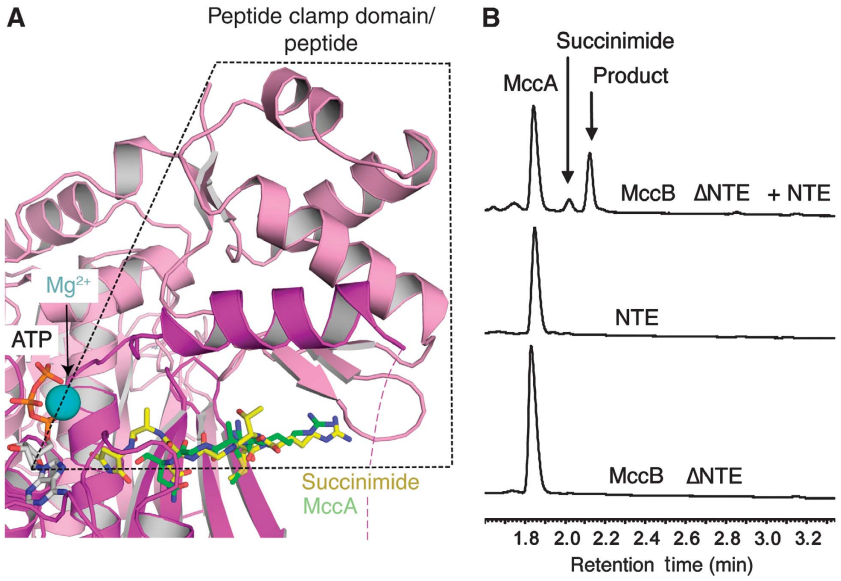

Figure 3 The unique MccB peptide clamp domain required for activity. (**A**) Close-up view of the MccB-binding site for peptide substrates. Structural superposition of MccB–MccA, (only MccA shown), MccB–succinimide, and MccB–MgATP (only MgATP shown). The two protomers in the MccB homodimer are shown in cartoon representation in pink and magenta. MccA, the succinimide intermediate, and ATP are depicted as sticks, with their carbon atoms in green, yellow, and grey, respectively. Nitrogen atoms are shown in blue, oxygen atoms in red, and phosphorous atoms in orange. The Mg^{2+} ion is shown as a cyan sphere. The MccB peptide clamp domain and associated peptide substrates are located inside the dotted box. (**B**) The separately expressed NTE of MccB (NTE) rescues the activity of truncation mutants lacking the NTE (ΔNTE). HPLC traces (220 nm) showing the product resulting from incubation of MccA with MccB ΔNTE (10 μM), isolated NTE (100 μM), or both in reaction buffer for 2 h at room temperature.

the C-terminus of the succinimide peptide comes close to approaching the adenylation-active site. In the crystals, the C-terminus of the peptide substrate MccA occupies several locations, none of which is as close to the adenylation-active site as the succinimide. A different backbone conformation is observed for the MccA–N7isoAsn inhibitor, which is a subtle variant of the first-peptide substrate. Residues Thr_3-Asn_5 of the inhibitor are 'looped out' by one residue relative to the corresponding substrate structures, such that the Ala_6-$isoAsn_7$ backbone aligns with Asn_5-Ala_6 from the succinimide peptide. Thus, the C-terminus of MccA–N7isoAsn does not come as close to the adenylation-active site as the succinimide peptide. The conformational variability observed at the C-termini of the peptides will be discussed below.

Comparison of the peptide-MccB structures with UBLs complexed with their activating enzymes (Lake *et al*, 2001; Walden *et al*, 2003a; Lois and Lima, 2005; Lehmann *et al*, 2006; Huang *et al*, 2007; Lee and Schindelin, 2008) reveals that the MccA-derived peptides resemble the last seven residues of E1-bound UBLs (Supplementary Figure 6). Thus, it seems that the unique MccB peptide clamping mechanisms direct substrates to an E1-like active site.

Adenylation-active site

ATP binds in a cleft centred around the MccB Gly-Cys-Gly-Gly-Ile-Gly nucleotide-binding motif, near the C-terminal end of the MccA-derived peptides. Many features of MccB's ATP-binding site resemble those of MoeB/ThiF and E1s, with both protomers in the MccB dimer contributing to the ATP-binding site (Figure 5A; Supplementary Figure 7) (Lake *et al*, 2001; Walden *et al*, 2003a; Duda *et al*, 2005; Lois and Lima, 2005; Huang *et al*, 2007). A hydrophobic pocket (L121, I194, A213, L219) binds ATP's adenine. Polar residues (N154, R157, Q158, K170) contact ATP's ribose and phosphates. An Arg finger (94) is provided by the opposite monomer in the complex. Mutation of the Arg finger to alanine (R94A) has no significant effect on the k_{cat}, but increases the K_m for both MccA and ATP (Table II).

Mg^{2+} is coordinated by the three ATP phosphates and D214. D214 is absolutely conserved as an Asp in all UBL-activating enzymes (Supplementary Figure 2). The corresponding Asp residue was shown earlier to be essential for catalysis by the UBL-activating enzymes *E. coli* MoeB and the human NEDD8 E1 (Lake *et al*, 2001; Walden *et al*, 2003b). Furthermore, mutation of the corresponding Asp in the ubiquitin E1, UBA1, had pleiotropic effects, including increasing the K_m for ATP and ubiquitin and decreasing the k_{cat} for many steps in ubiquitination (Tokgoz *et al*, 2006). The earlier studies on UBA1 support a dual function of the Asp in binding MgATP and transition state stabilization (Tokgoz *et al*, 2006). The MccB residue D214 is essential for catalysis; we were unable to detect conversion of MccA to succinimide or product by the D214A mutant. (Figure 5B). However, coincubation of the D214A and ΔNTE mutants with MccA yields activity similar to mixing the isolated NTE with the ΔNTE mutant (Supplementary Figure 8). The former result could either be explained by complementation in trans or by a low concentration of mixed dimers in which ΔNTE would contribute the catalytic D214, and the full-length version harbouring the D214A mutation would contribute a peptide clamp to form one complete-active site per heterodimer. In either case, the finding of limited activity indicates the importance of the adenylation-active site working in concert with the peptide clamp domain.

Unique features of the MccB-active site

In addition to the shared properties with E1s, the MccB Y239 stands out as being unique in the adenylation catalytic site.

Table II MccB mutants kinetics

Mutant	MccA			ATP		
	K_m (μM)	k_{cat} (h^{-1})	k_{cat}/K_m ($h^{-1}\,\mu M^{-1}$)	K_m (μM)	k_{cat} (h^{-1})	k_{cat}/K_m ($h^{-1}\,\mu M^{-1}$)
MccB (WT) (Roush *et al*, 2008)	61 ± 16	6.4 ± 1.8	0.1	70 ± 30	12.5 ± 2.4	0.18
MccB K10A	370 ± 240	2.8 ± 1.2	0.007	120 ± 20	3.7 ± 0.5	0.03
MccB R94A	950 ± 260	2.8 ± 1.9	0.003	380 ± 130	4.5 ± 3.3	0.008
MccB C123V	60 ± 15	6.0 ± 1.5	0.1	270 ± 140	7.0 ± 2.9	0.02
MccB C123L	49 ± 10	1.8 ± 0.3	0.04	220 ± 80	1.1 ± 0.3	0.008
MccB D214A		—*Not active*—			—*Not active*—	
MccB H215A	100 ± 40	5.6 ± 2.3	0.05	150 ± 40	7.5 ± 2.6	0.05
MccB Y239A	250 ± 70	0.01 ± 0.006	0.00003	380 ± 190	0.02 ± 0.008	0.00005
MccB N241A	440 ± 140	0.8 ± 0.4	0.002	400 ± 120	1.7 ± 0.5	0.004
MccB ΔNTE + NTE	700 ± 200	1.1 ± 0.4	0.002	3800 ± 1900	2.9 ± 1.2	0.0007
MccB ΔNTE		—*Not active*—			—*Not active*—	
MccB NTE		—*Not active*—			—*Not active*—	

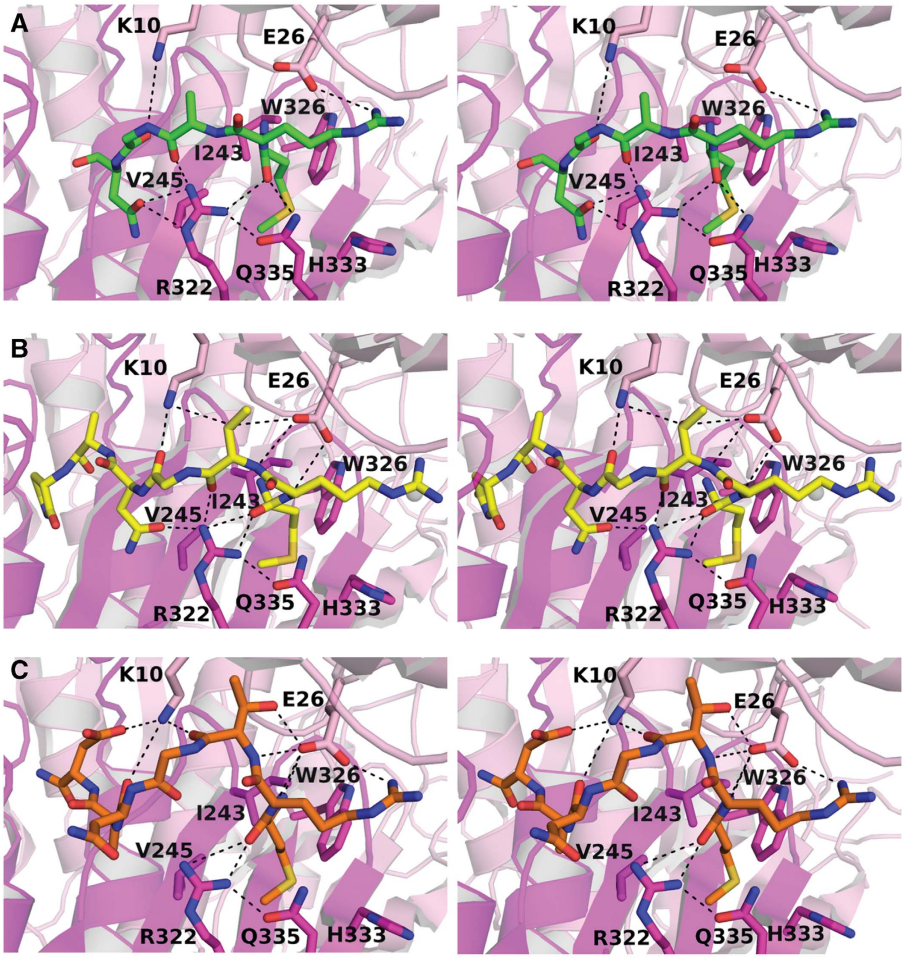

Figure 4 MccB binding to MccA. Stereo panels showing contacts between MccB and the MccA peptide ligands. The two protomers in the MccB homodimer are shown in cartoon representation in pink and magenta. MccB side chains and peptides are depicted as sticks, and contacts within 5 Å are indicated by dashes. (**A**) MccA, green. (**B**) MccA–succinimide, yellow. (**C**) MccA–N7isoAsn, orange. Nitrogen atoms are shown in blue and oxygens in red.

Y239 contacts both the ATP α-phosphate and the heptapeptide substrate C-terminus (Figure 5A). Y239 is located on the opposite side of MccA from the Mg^{2+}-coordinating D214. Together, Y239 and D214 seem to form a bridge. The MccA and succinimide peptide substrates would need to pass into a channel under the D214–Y239 bridge for adenylation. Y239 has an important catalytic role, as illustrated by the ~five-fold increase in K_m for both ATP and MccA and >600-fold decrease in k_{cat} in the Y239A mutant (Table II; Figure 5C).

Notably, the MccA C-terminus is atypical among substrates of UBL-activating enzymes as not terminating in the sequence Gly-Gly. Structural comparison reveals that UBL penultimate Glys are oriented by a key E1 Arg, which is lacking and substituted with I220 in MccB. MccB's aforemen-

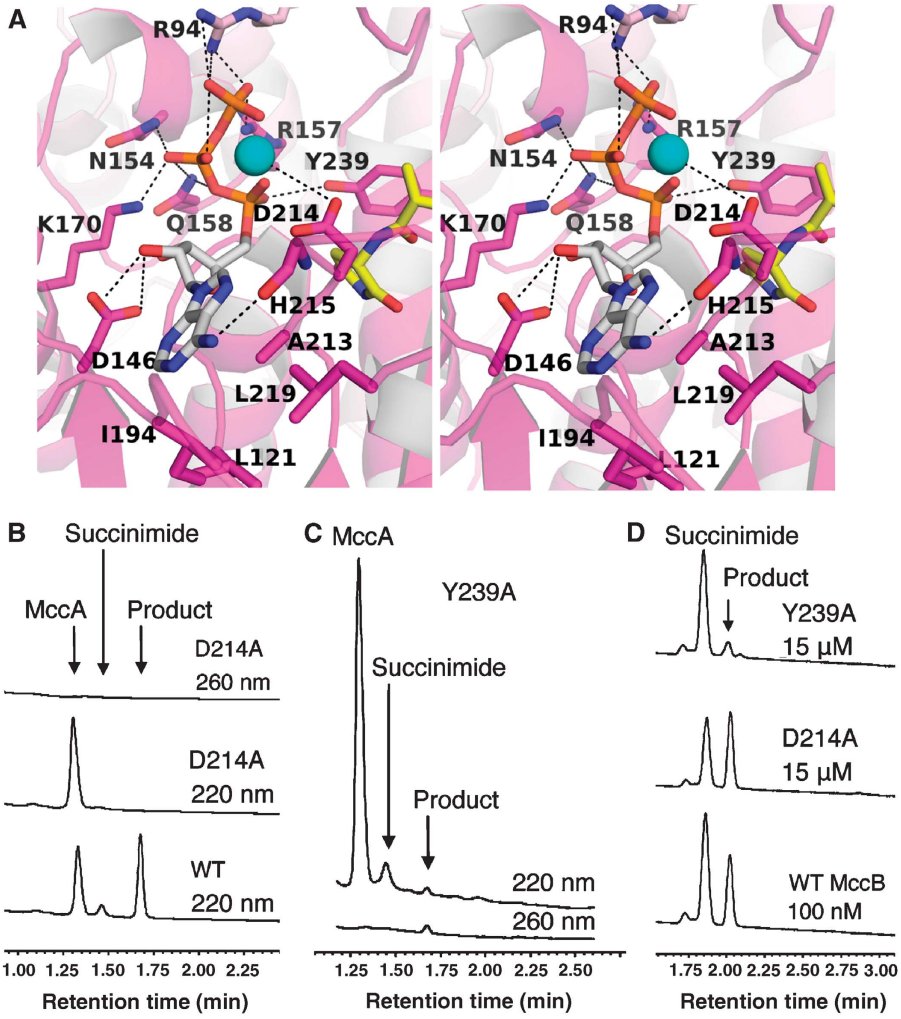

Figure 5 A common adenylation-active site for MccA and MccA–succinimide. (**A**) Close-up views of the MccB adenylation-active site is shown in stereo. The MccB–MgATP structure is shown, with the succinimide intermediate modelled after structural superposition of MccB–MgATP and MccB–succinimide complexes. MccB is depicted as in Figure 2 with side chains shown as sticks, and contacts within 5 Å indicated by dashes. (**B**) MccB D214A is unable to catalyse generation of the succinimide intermediate or product from MccA. HPLC traces (220 and 260 nm) showing lack of product formation after incubation of MccA and ATP with MccB D214A in reaction buffer for 5 h at room temperature. Further incubation to 24 h gave no product. (**C**) The MccB Y239A mutation significantly hinders enzymatic activity for reactions starting with MccA. HPLC traces (220 and 260 nm) showing the product resulting from incubation of MccA with MccB–Y239A (10.5 μM) in reaction buffer for 24 h at room temperature. (**D**) MccB D214A and Y239A are defective at converting the succinimide to product. HPLC traces (220 nm) showing incubations of WT MccB (100 nM), MccB–D214A (15 μM), or MccB–Y239A (15 μM) mutants with 100 μM MccA–succinimide in reaction buffer for 3.5 h at room temperature.

tioned unique Y239 may also prevent Gly-Gly recognition. The corresponding E1 residue is a small Ala or Thr, which allows proper orientation of a UBL C-terminal Gly-Gly. In contrast, the MccB adenylation-active site is slightly displaced as compared with UBL-activating enzymes, with Y239 altering the conformation of the MccA-contacting β-strand13, and obscuring the path taken by a UBL Gly-Gly (Supplementary Figure 9). The channel leading under the D214–Y239 bridge and towards ATP is lined with backbone hydroxyls, which may also favour binding to MccA's C-terminal Asn, and prevent binding of closely related peptides as observed for MccA-N7D (Roush *et al*, 2008).

Successive adenylation reactions at a common-active site

A striking feature of the MccB mechanism is the usage of two ATP molecules per catalytic cycle: one for the adenylation of MccA and the second for the formation of the N–P bond through the adenylation of the succinimide intermediate (Roush *et al*, 2008). The mutants D214A and Y239A have significant reductions in overall turnover (Figure 5B and C); we were unable to detect any product formation by D214A starting from the heptapeptide substrate MccA (Figure 5B). The structural data suggests that there is one common-active site for MccA and the succinimide intermediate, so we therefore evaluated the processing for the synthetic peptidyl-succinimide intermediate on the second half reaction with our most deleterious point mutants, D214A and Y239A. The detection limit for high-performance liquid chromatography (HPLC) assays was 10 pmol of MccB product, which amounted to a rate of 0.01% of WT enzyme over a 24-h time period. The conversion of the succinimide intermediate to product, representing the second ATP consumption step, occurs 40 times faster than

the overall reaction starting with MccA (Roush *et al*, 2008). Therefore, assaying the mutants with the succinimide intermediate is more sensitive. On incubation of WT MccB (0.1 μM), or the D214A or Y239A mutants at 150-fold higher enzyme concentrations (15 μM) to magnify sensitivity with 100 μM peptidyl-succinimide, product formation was detected (Figure 5D). D214A was ~150-fold slower than WT, and Y239A was ~600-fold slower than WT MccB in this second half reaction.

Therefore, the D214A and Y239A mutations markedly affect both overall turnover and the peptidyl-succinimide to acyl-phosphoramidate product step. As the peptidyl-succinimide does not accumulate in assays of D214A and Y239A starting with MccA (data not shown), we intuit that both the first and the second ATP-using steps are slowed down more than two orders of magnitude and that the formation of the heptapeptidyl-AMP, the cyclization to the succinimide, and the rearrangement to the final N–P-linked product occur in the same active site.

Conformational variability of MccB, MccA-derived heptapeptides, and nucleotide

Comparing the different structures reveals that all three components—MccB, MccA, and nucleotide—display conformational variability (Figure 6). MccB conformational flexibility occurs both at a global and a local level. Superposition of the adenylation domains of the different structures reveals that the adenylation and peptide clamp domains can adopt a range of orientations with respect to each other, opening and closing as for two halves of a clamshell (Figure 6A). Despite this flexibility, there are many connections between the two domains. As an example, N241 projects away from the MccB adenylation domain to coordinate with the location of peptide clamp domain. This link has a function in the reaction as substitution with Ala decreases k_{cat} five-fold and increases K_m ~six-fold for both MccA and ATP (Supplementary Tables I–III).

There is also extensive local flexibility at the adenylation-active site. Side-chain positions of ATP-binding residues, such

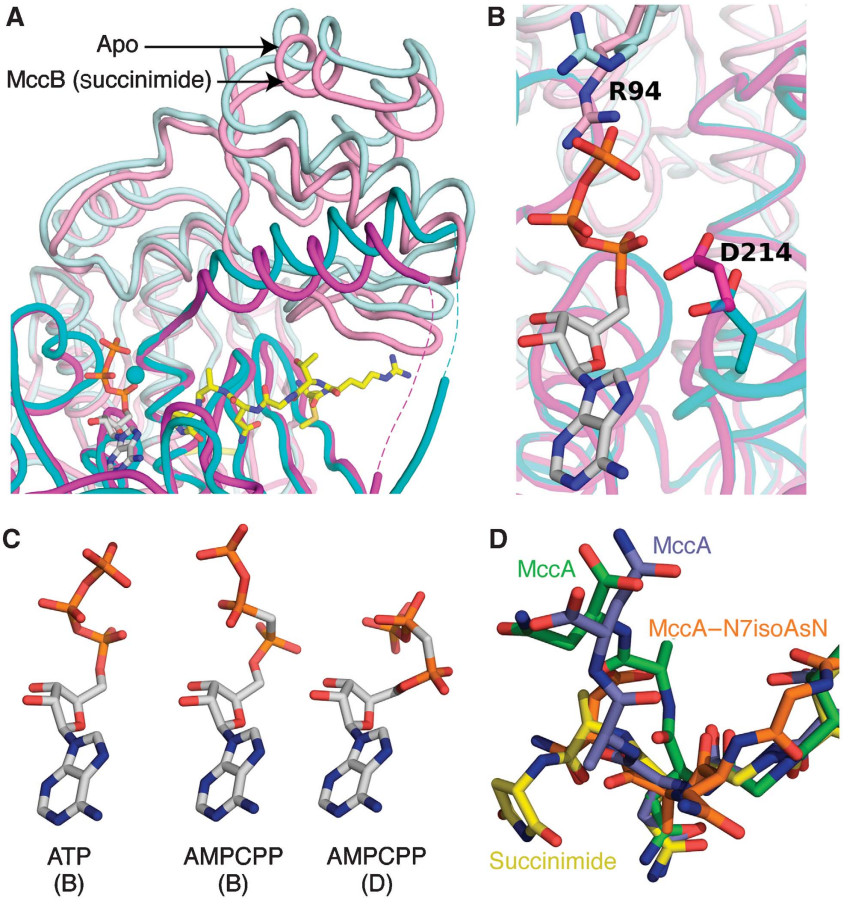

Figure 6 Conformational flexibility of MccB, MccA, and nucleotide substrates. (**A**) Structures of free MccB and the MccB–succinimide complex are shown superimposed over the adenylation domain, with the two protomers in each structure coloured in dark cyan/light cyan or magenta/pink, respectively. Locations of parallel portions of the peptide clamp domains from the two structures are indicated. MgATP is modelled into the adenylation-active site based on superposition of the MccB–MgATP structure. The MccB backbone is depicted as a tube, Mg^{2+} ion is shown as a cyan sphere, and succinimide and ATP are shown as yellow and grey sticks, respectively. Nitrogen atoms are shown in blue, oxygen atoms in red, and phosphorous atoms in orange. (**B**) MccB side-chain flexibility in the adenylation-active site. Structures of MccB–ATP and MccB–succinimide complex are shown superimposed, with the two protomers in each structure coloured in dark cyan/light cyan or magenta/pink, respectively. Side chains from the ATP-binding residue R94 and key catalytic residue D214 are depicted as sticks, with the MccB backbone depicted in transparent tube. (**C**) Conformations of ATP and the nucleotide analogue AMPCCP from the indicated chains in complexes with MccB. (**D**) Conformations of the C-terminal portion of MccB's peptide substrates, depicted as sticks, with carbon atoms from MccA in complex with MccB in green, from MccA in complex with MccB–AMPCPP in blue, from MccA–succinimide in complex with MccB in yellow, and from MccA–N7isoAsn in complex with MccB in orange.

as R94, and a key catalytic residue, the Mg^{2+}-coordinating D214, vary considerably between structures (Figure 6B). The nucleotide ligands also adopt a range of conformations within the active site. Although the adenine and ribose moieties superimpose well (RMSD ~0.5 Å), the relative locations of the three phosphates in AMPCPP differ from ATP, and between distinct AMPCPP molecules in the asymmetric unit (Figure 6C).

The peptide structures also show striking conformational variability. In each MccA complex, the C-terminus is not visible for at least one peptide in the asymmetric unit (see Materials and methods). When the C-terminus is present, it is not directed towards the adenylation active site. Thus, the Cα positions of the succinimide and MccA's C-terminus in structures with or without AMPCPP differ by ~8 Å (Figure 6D). The ability of MccB to bind substrate peptides with a range of conformations, anchored by their N-terminus and backbone carbonyls, likely explains why *in vivo* substitutions for MccA's residues 2, 4–6 are tolerated for the production of a complete MccC7 variant, but few are accepted for T_3 (Kazakov *et al*, 2007).

The peptide C-terminal flexibility was unexpected and may be a unique feature of the MccB–MccA system when compared with UBL-activating enzymes. For each of the five structurally determined UBL-activating enzyme complexes, there are 2–21 independent UBL models that superimpose well at their C-termini (Lake *et al*, 2001; Walden *et al*, 2003a; Lois and Lima, 2005; Lehmann *et al*, 2006; Huang *et al*, 2007; Lee and Schindelin, 2008; Souphron *et al*, 2008), and they also superimpose well for the complexes from different pathways. Further studies will be necessary to reveal whether UBL C-termini also display such conformational flexibility in complexes with their activating enzymes, or whether this is a unique feature of the MccB–MccA system.

E1-like protein that functions without forming a thioester or an acyl-disulfide intermediate

UBL-activating enzymes generally catalyse multiple reactions. After UBL adenylation, subsequent reactions often involve formation of a covalent UBL~enzyme complex, such as a thioester or acyl-disulfide intermediate linked through an activating enzyme thiol (Ciechanover *et al*, 1981; Haas and Rose, 1982; Haas *et al*, 1982; Haas and Siepmann, 1997; Johnson *et al*, 1997; Xi *et al*, 2001; Bohnsack and Haas, 2003; Pickart and Eddins, 2004), although neither *E. coli* MoeB nor ThiF from some organisms require such a covalent enzyme–UBL intermediate (Leimkuhler *et al*, 2001; Park *et al*, 2003). To explore the possibility of an acyl-S-enzyme intermediate for MccB, all cysteines not involved in zinc binding (Cys residues 44, 68, 123, 227 and 302) were mutated to alanines (Supplementary Figure 10A). No MccB Cys is essential for catalysis. One Cys, C123, is located in the Gly-Cys-Gly-Gly-Ile-Gly Walker A motif (Walker *et al*, 1982), and thus seems to have a structural function in establishing the nucleotide-binding site (Figure 7). In other UBL-activating enzymes, the residue corresponding to C123 is either a Leu or a Val, so, therefore, the C123V and C123L mutants were considered. All Cys mutants had similar activity profiles to the WT enzyme (Supplementary Figure 10B) with the exception of C123L and C123V. Conversion of C123 to bulkier, hydrophobic residues caused the succinimide intermediate to be present

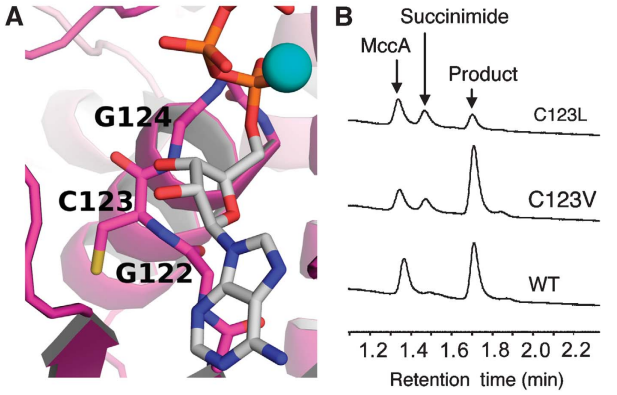

Figure 7 A structural role for the only non-zinc-binding Cys important for MccB activity. (**A**) Close-up view of the MccB structure showing the location of C123 in the Gly-Cys-Gly-Gly-Ile-Gly Walker A nucleotide-binding motif of MccB. (**B**) MccB C123L and C123V mutants have an alternate activity profile when compared with WT MccB. HPLC traces (220 nm) showing the product resulting from incubations of MccA with WT MccB or indicated mutant (2.5 μM) in reaction buffer for 3 h at room temperature.

at higher levels than in reactions with the WT enzyme. Mutation of C123 to a bulkier Leu impaired activity (Figure 7B; Table II). Consistent with the structurally important role of C123, iodoacetamide is inactivating, likely due to an indirect effect on the structure of the adenylation-active site (Figure 7; Supplementary Figure 10). Thus, unlike E1s and the prokaryotic UBL-activating enzyme ThiF (Xi *et al*, 2001), MccB function does not require thiol-mediated catalysis. Intramolecular capture of the nascent peptidyl-AMP is the only kinetically significant outcome.

Prokaryotic variations on E1–UBL themes

Prokaryotic UBL–E1-like complexes, ThiS–ThiF and MoaD–MoeB, have long been recognized for their roles in sulphur incorporation into thiazole and molybdopterin, respectively (Rajagopalan, 1997; Begley *et al*, 1999). Both ThiS and MoaD structurally resemble UBLs, and are activated by ThiF or MoeB-catalysed adenylation of their C-terminal Gly-Gly sequences. ThiF and MoeB consist exclusively of an adenylation domain (Lake *et al*, 2001; Duda *et al*, 2005; Lehmann *et al*, 2006), and thus represent minimal modules harbouring UBL recognition and adenylation activities.

The structures of MccB reveal four key features that functionally distinguish its unique properties relative to ThiF, MoeB, and all other UBL-activating enzyme family members. The first two define MccB as a modifier of peptide, and not of a UBL: (1) the ~100-residue NTE and (2) an extended crossover loop sequence together form the peptide clamp domain. The second two define MccB as *NOT* recognizing a C-terminal Gly-Gly motif: (3) the lack of a conserved Arg at MccB's position I220 and (4) the D214–Y239 bridge (Y239 being unique to MccB). This latter characteristic may also contribute to MccB's selectivity for a C-terminal Asn. Interestingly, these features define a large clade of the UBL-activating enzyme family. Database searches revealed that numerous bacterial species have proteins sharing all these hallmark features of MccB (Severinov *et al*, 2007). Furthermore, potential paralogues of MccA and downstream components of the MccC7 biosynthetic pathway have also been identified in these same organisms. Notably, relative to

the active site sequences, the anticipated peptide-binding residues are poorly conserved among the MccB homologues, and the MccA paralogues also display a range of sequences, while maintaining a C-terminal Asn. Although these enzymes remain uncharacterized, it seems likely that the MccB-like enzymes from many bacteria use a range of starting peptide sequences to generate phosphoramidate-linked analogues of aspartic acid acyl-adenylate.

A recent study identified a novel Mycobacterial UBL, Pup, which like ubiquitin becomes C-terminally conjugated to a target's Lys through an isopeptide linkage (Pearce *et al*, 2008). Similar to MccA, Pup's C-terminal residue is not a Gly, but rather a Gln that seems to undergo deamidation during conjugation. No E1 has been identified for Pup. Thus, it seems that prokaryotes use a wide array of variations of UBLs, E1s, or both not only for sulphur incorporation in biosynthetic pathways, but also for a range of posttranslational modifications of proteins (e.g. pupylation) and of peptides for conversion to antibiotics.

Implications for MccB-catalysed production of a phosphoramidate-linked analogue of aspartic acid acyl-adenylate

Our structural and biochemical data yielded several insights into a unique member of the UBL-activating enzyme family. MccB can use peptide substrates by virtue of a novel and essential peptide clamp domain. The clamp works in concert with the opposing surface, which is the adenylation domain. Despite similarities to the adenylation-active sites of UBL-activating enzymes, MccB catalyses two adenylation reactions: first on a C-terminal Asn and subsequently on a succinimide moiety to form an N–P bond. Both substrates are directed towards the active site for attack on the ATP α-phosphate and consequent adenylation. The D214A and Y239A mutants are significantly impaired in converting both the first- and second-peptide substrates to product; a single mutation hinders both adenylation events. In our crystal structures, these residues are poised near the ATP α-phosphate to position the substrate C-termini for adenylation. Therefore, it seems that each adenylation occurs within the same active site.

Although none of the structurally observed peptide C-termini are positioned for catalysis, a catalytically relevant model for the final reaction can be generated by subtle substrate peptide rearrangements. Rotation about the succinimide C–N bond ~180° reduces the catalytic gap within 4 Å (Figure 8). The model is consistent with a mechanism, whereby the MccB Y239 and the Mg^{2+} ion coordinated by MccB's D214 orient the ATP α-phosphate. On the basis of their relative locations to the α-phosphate, we speculate that D214 and Y239 may form a bridge that positions the MccA C-terminus for the initial reaction. With the Mg^{2+} ion relieving electrostatic repulsion, the MccA C-terminal carboxylate oxygen can first attack the ATP α-phosphate. The Mg^{2+} ion and side chains from MccB R157, Q158, and K170 are poised to stabilize a developing negative charge on the ATP β-phosphate in the anticipated transient pentacovalent phosphate species, allowing resolution to MccA-peptidyl-adenylate and inorganic pyrophosphate.

Subsequent steps in this antibiotic biosynthetic mechanism are exclusive to MccB, and are not shared by UBL-activating enzymes. The MccB structures reveal features that can accommodate the unique proceeding chemical steps on the nascent peptidyl-AMP. The structurally observed local flexibility at the adenylation-active site likely facilitates having multiple catalytic events occur there after the initial adenylation reaction. These events include the intramolecular closure of the Asn_7 carboxamido nitrogen on the –CO-AMP moiety and collapse of the tetrahedral adduct to expel AMP to generate the succinimide intermediate. This may be released from the enzyme or, given the peptide clamp domain, may react with a second molecule of ATP before dissociation. Exogenous peptidyl-succinimide is chemically and kinetically competent as an intermediate for MccB conversion to the N-P-AMP final product, so that the 'off' and 'on' steps can be fast relative to the second adenylation.

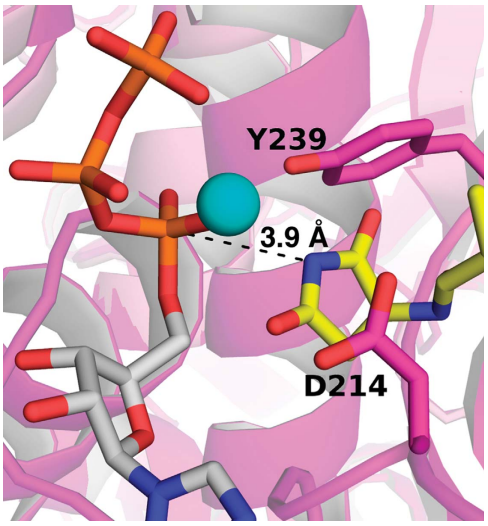

Figure 8 Rotation of the succinimide about the C–N bond may position the intermediate for catalysis. An ~180° rotation about the structurally observed succinimide group allows proximity to the ATP α-phosphate, allowing a model for a putative catalytic intermediate.

The most remarkable chemical transformation catalysed by MccB is the subsequent transfer of AMP to the succinimido nitrogen. We propose that placement of the peptidyl-succinimide in the active site, secured by MccB's unique peptide clamp, orients the succinimide nitrogen to attack another molecule of ATP that has diffused into the active site. Thus, the peptide clamp domain would allow two adenylation reactions to be performed sequentially: the first with a typical peptide-C-terminal carboxylate oxygen as nucleophile and the second with the succinimide nitrogen as nucleophile. In the proposed mechanism, two canonically weak nucleophiles within the substrate framework are competent. The first is the entropically favoured intramolecular cyclization of the Asn_7 β-carboxamide N on Cα of the peptidyl-AMP nascent product. The second is the intermolecular reaction of the cyclic succinimido nitrogen of Pα of another bound ATP, which creates the unusual N–P linkage that is the hydrolytically stable centrepiece of the antibiotic maturation logic.

Materials and methods

Purification of MccB proteins for activity assays and crystallography

For activity assays, MccB and variants were prepared as described earlier (Supplementary data) (Roush *et al*, 2008). Preparation of

MccB truncation mutants included a thrombin cleavage step. For crystallographic studies, MccB with a C-terminal His_6-tag and a cleavable, N-terminal His_6-tag were purified by Ni^{2+} affinity, anion exchange, and gel filtration chromatography in 20 mM Tris pH 8.0, 150 mM NaCl, and 5 mM DTT. Preparation of MccB lacking the N-terminal His_6-tag included a thrombin cleavage step after affinity purification. MccB was concentrated to 25–28 mg/ml by ultrafiltration at 4°C, aliquoted, flash frozen, and stored at −80°C. Peptides for crystallography were synthesized and reverse-phase HPLC purified by the Hartwell Center for Bioinformatics and Biotechnology at St Jude.

Crystallization and data collection

Crystals of MccB-His_6 were grown by hanging drop vapour diffusion at 4°C in 100 mM Tris pH 8.0, 2.1 M $NaCl_2$, cryoprotected in the mother liquor supplemented with increasing concentrations of glycerol in four steps from 10 to 40% (v/v), and flash frozen in liquid nitrogen for data collection. These crystals form in the space group $P2_12_12_1$ with two MccB homodimers in the asymmetric unit. The MccB-His_6 dimers packed so that the C-terminal His_6-tag of protomers A and C passed under the crossover loops of adjacent protomers D and B, respectively. To prevent a His_6-tag from interfering with the crossover loop for all complex structures, MccB produced with a cleavable and removed N-terminal His_6-tag was crystallized. Screens produced crystals in several conditions at 4 and 18°C. Crystals in space group $P2_1$ were grown at 18°C by microseeding, with two MccB homodimers per asymmetric unit. The well condition varied depending on the complex; the precipitant was 24–26% pentaerythritol ethoxylate (15/4 EO/OH, Hampton Research). Additional components of each crystallization condition are as follows: MccB(MccA–N7isoAsn): 50 mM Tris pH 8.0, 50 mM $(NH_4)_2SO_4$, 10 mM MccA–N7isoAsn; MccB(MccA): 50 mM Bis–Tris pH 6.5, 50 mM $(NH_4)_2SO_4$, 10 mM SeMet-MccA; MccB(succinimide): 50 mM Bis–Tris pH 6.5, 50 mM $(NH_4)_2SO_4$, 10 mM succinimidyl peptide; MccB(ATP): 50 mM Na Hepes pH 7.5, 100 mM $MgSO_4$, 25 mM ATP; MccB(MccA–AMPCPP): 50 mM Na Hepes pH 7.5, 100 mM $MgSO_4$, 9 mM α,β-methyleneadenosine 5′-triphosphate (AMPCPP) (SIGMA, catalogue #M6517), 9 mM SeMet-MccA.

Pentaerythritol ethoxylate was a suitable cryoprotectant, so crystals were flash frozen after harvesting directly from the drop. For MccB(MccA–N7isoAsn) and MccB(succinimide), the crystals were soaked in 30% pentaerythritol ethoxylate supplemented with the buffer and additives at the same concentration as in the well, and a higher concentration of peptide ligand, 60 and 20 mM, respectively.

Reflection data were collected at beamlines 8.2.1 and 8.2.2 at The Advanced Light Source and SERCAT 22-ID, 22-BM, and NECAT 24-ID at The Advanced Photon Source and were processed with HKL2000 (Otwinowski and Minor, 1997).

Structure determination, refinement, and analysis

The crystal structure of MccB-His_6 (Apo) was determined to 2.8 Å by three-wavelength Zinc-MAD (Table I). Four Zn^{2+} sites were located and refined using the program SOLVE (Terwilliger and Berendzen, 1999). The final Z-score and figure of merit were 30.0 and 0.28, respectively. Density modification of phases from SOLVE was performed with RESOLVE (Terwilliger, 2000), yielding maps with continuous electron density from the N- to C-termini. The apo model was built manually using the ThiF model as a guide (PDB 1ZFN; Duda *et al*, 2005) in COOT (Emsley and Cowtan, 2004) and refined against the peak dataset using restrained refinement in REFMAC5 (Murshudov *et al*, 1997), with 5% of the reflections set aside as the test set. Placement of side chains was verified with simulated-annealing composite-omit maps calculated with central nervous system (CNS) (Brunger *et al*, 1998).

MccB(MccA–N7isoAsn) was determined by molecular replacement with PHASER (McCoy *et al*, 2007) using the apo dimers A–B and C–D, lacking crossover loops as independent search models. Subsequent complex structures were determined by rigid-body refinement with REFMAC5 using the MccB(MccA–N7isoAsn) structure lacking the peptide, solvent, and crossover loops. Each asymmetric unit can contain four peptides (two for each dimer), and in all structures the N-terminal Met or SeMet was observed in F_o–F_c maps contoured at 3 σ. In addition, the anomalous signal from SeMet-MccA was used to verify the location of the N-terminus of the peptide; 10 σ peaks for the SeMet were observed in anomalous maps (Supplementary Figure 3A). Density extended beyond the N-terminal Met or SeMet for a minimum of one peptide within the asymmetric unit, so that each structure contains at least one peptide modelled from the N- to C-termini. Peptides that were not built completely are truncated. For the nucleotide-bound structures, all four cofactors are modelled. There seems to be a high propensity for anion binding to this region, as additional electron density in the MccB–MccA–N7isoAsn structure localizes to the same relative location as ATP's α-phosphate. We modelled this density as sulphate from $NH_4(SO_4)_2$ in the crystallization solution. Complex structures were refined with REFMAC5 (Murshudov *et al*, 1997) using TLS or CNS (Brunger *et al*, 1998) with the same set of reflections set aside as the test set to avoid biasing the R_{free}. For analysis, all A–B and C–D dimers were superimposed with MultiProt (Shatsky *et al*, 2004).

MccB activity assays

Peptides were synthesized through solid-phase peptide synthesis by staff at the Biopolymers Facility, Department of Biochemistry and Molecular Pharmacology, Harvard Medical School, Boston, MA. Their purity and identities were confirmed by HPLC/LCMS. MccA and MccA–N7isoAsn have the sequences MRTGNAN and MRTGNAisoN, respectively. The succinimidyl peptide (MRTGNA-succinimide) was synthesized as described earlier (Novoa *et al*, 1986; Roush *et al*, 2008).

MccB was incubated with MccA (250 μM) in reaction buffer (75 mM Tris–HCl pH 8.0, 5 mM $MgCl_2$, 2.5 mM TCEP, 5 mM ATP). Reactions were quenched by addition of equal volume of 0.6% TFA/H_2O. Product formation was monitored by analytical HPLC using a gradient of 0–40% B in 8 min with a flow rate of 4 ml/min (solvent A: 0.1% TFA in H_2O; solvent B: acetonitrile). For a list of all mutants tested, see Supplementary Table I.

Iodoacetamide inactivation of MccB

MccB (5 μM) was incubated in buffer (75 mM Tris–HCl, 5 mM $MgCl_2$) with or without iodoacetamide (5 mM) at 37°C for 1 h. Unreacted iodoacetamide was quenched by the addition of 10 mM dithiothreitol. Product formation was monitored after incubation with ATP (5 mM) and MccA (250 μM) at room temperature for 1.5 h.

Kinetic characterization of the MccB-catalysed reaction

The detection limit for HPLC assays was 10 pmol of MccB product, which amounted to a rate of 0.01% of WT enzyme over a 24-h time period. Kinetic investigations were conducted in buffer (75 mM Tris–HCl pH 8.0, 5 mM $MgCl_2$, 2.5 mM TCEP). The 100-μl reactions were quenched with equal volume of 0.6% TFA/H_2O, and product formation was monitored by analytical HPLC. Product peaks (260 nm) were integrated and the resulting values were converted to molecules formed by using an ATP standard curve (62.5–500 μM ATP). Data were fit to the Lineweaver–Burk equation in Microsoft Excel and reported values are the mean ± standard deviation of at least three independent trials. For the range of concentrations tested, see Supplementary Tables II and III.

Accession codes

The coordinates and structure factors have been deposited in the RCSB with the following accession codes: 3H5A Apo, 3H57 MccB(MgATP), 3H9G MccB(MccA-N7isoAsn), 3H9Q MccB(MccA), 3H9J MccB(MccA-AMPCPP), 3H5R MccB(Succinimide).

Supplementary data

Supplementary data are available at *The EMBO Journal* Online (http://www.embojournal.org).

Acknowledgements

We thank Elizabeth Nolan and Michael Fischbach for helpful discussions. This work was supported in part by ALSAC (American Syrian Lebanese Associated Charities), grants from the NIH (RO1GM49338 to CTW, R01GM069530 to BAS, F32CA136121 to CAR, P30CA021765 to St Jude Cancer Center), and by the Howard Hughes Medical Institute. BAS is an Investigator of the Howard Hughes Medical Institute. The Advanced Light Source is supported by the Director, Office of Science, Office of Basic Energy Sciences, the US Department of Energy under Contract No. DE-AC02-05CH11231, and the Advanced Photon Source under Contract No. W-31-109-Eng-38.

References

Begley TP, Xi J, Kinsland C, Taylor S, McLafferty F (1999) The enzymology of sulfur activation during thiamin and biotin biosynthesis. *Curr Opin Chem Biol* **3:** 623–629

Bohnsack RN, Haas AL (2003) Conservation in the mechanism of Nedd8 activation by the human AppBp1-Uba3 heterodimer. *J Biol Chem* **278:** 26823–26830

Brunger AT, Adams PD, Clore GM, DeLano WL, Gros P, Grosse-Kunstleve RW, Jiang JS, Kuszewski J, Nilges M, Pannu NS, Read RJ, Rice LM, Simonson T, Warren GL (1998) Crystallography & NMR system: a new software suite for macromolecular structure determination. *Acta Crystallogr D Biol Crystallogr* **54:** 905–921

Ciechanover A, Heller H, Katz-Etzion R, Hershko A (1981) Activation of the heat-stable polypeptide of the ATP-dependent proteolytic system. *Proc Natl Acad Sci USA* **78:** 761–765

Duda DM, Walden H, Sfondouris J, Schulman BA (2005) Structural analysis of Escherichia coli ThiF. *J Mol Biol* **349:** 774–786

Duquesne S, Petit V, Peduzzi J, Rebuffat S (2007) Structural and functional diversity of microcins, gene-encoded antibacterial peptides from enterobacteria. *J Mol Microbiol Biotechnol* **13:** 200–209

Emsley P, Cowtan K (2004) Coot: model-building tools for molecular graphics. *Acta Crystallogr D Biol Crystallogr* **60:** 2126–2132

Guijarro JI, Gonzalez-Pastor JE, Baleux F, San Millan JL, Castilla MA, Rico M, Moreno F, Delepierre M (1995) Chemical structure and translation inhibition studies of the antibiotic microcin C7. *J Biol Chem* **270:** 23520–23532

Haas AL, Rose IA (1982) The mechanism of ubiquitin activating enzyme. A kinetic and equilibrium analysis. *J Biol Chem* **257:** 10329–10337

Haas AL, Siepmann TJ (1997) Pathways of ubiquitin conjugation. *FASEB J* **11:** 1257–1268

Haas AL, Warms JV, Hershko A, Rose IA (1982) Ubiquitin-activating enzyme. Mechanism and role in protein-ubiquitin conjugation. *J Biol Chem* **257:** 2543–2548

Hochstrasser M (2000) Evolution and function of ubiquitin-like protein-conjugation systems. *Nat Cell Biol* **2:** E153–E157

Hochstrasser M (2009) Origin and function of ubiquitin-like proteins. *Nature* **458:** 422–429

Huang DT, Hunt HW, Zhuang M, Ohi MD, Holton JM, Schulman BA (2007) Basis for a ubiquitin-like protein thioester switch toggling E1-E2 affinity. *Nature* **445:** 394–398

Johnson ES, Schwienhorst I, Dohmen RJ, Blobel G (1997) The ubiquitin-like protein Smt3p is activated for conjugation to other proteins by an Aos1p/Uba2p heterodimer. *EMBO J* **16:** 5509–5519

Kazakov T, Metlitskaya A, Severinov K (2007) Amino acid residues required for maturation, cell uptake, and processing of translation inhibitor microcin C. *J Bacteriol* **189:** 2114–2118

Lake MW, Wuebbens MM, Rajagopalan KV, Schindelin H (2001) Mechanism of ubiquitin activation revealed by the structure of a bacterial MoeB-MoaD complex. *Nature* **414:** 325–329

Lee I, Schindelin H (2008) Structural insights into E1-catalyzed ubiquitin activation and transfer to conjugating enzymes. *Cell* **134:** 268–278

Lehmann C, Begley TP, Ealick SE (2006) Structure of the Escherichia coli ThiS-ThiF complex, a key component of the sulfur transfer system in thiamin biosynthesis. *Biochemistry* **45:** 11–19

Leimkuhler S, Wuebbens MM, Rajagopalan KV (2001) Characterization of Escherichia coli MoeB and its involvement in the activation of molybdopterin synthase for the biosynthesis of the molybdenum cofactor. *J Biol Chem* **276:** 34695–34701

Lois LM, Lima CD (2005) Structures of the SUMO E1 provide mechanistic insights into SUMO activation and E2 recruitment to E1. *EMBO J* **24:** 439–451

McCoy AJ, Grosse-Kunstleve RW, Adams PD, Winn MD, Storoni LC, Read RJ (2007) Phaser crystallographic software. *J Appl Cryst* **40:** 17

Metlitskaya A, Kazakov T, Kommer A, Pavlova O, Praetorius-Ibba M, Ibba M, Krasheninnikov I, Kolb V, Khmel I, Severinov K (2006) Aspartyl-tRNA synthetase is the target of peptide nucleotide antibiotic Microcin C. *J Biol Chem* **281:** 18033–18042

Mootz HD, Schwarzer D, Marahiel MA (2002) Ways of assembling complex natural products on modular nonribosomal peptide synthetases. *Chembiochem* **3:** 490–504

Murshudov GN, Vagin AA, Dodson EJ (1997) Refinement of macromolecular structures by the maximum-likelihood method. *Acta Crystallogr D Biol Crystallogr* **53:** 240–255

Nolan EM, Walsh CT (2008) Investigations of the MceIJ-catalyzed posttranslational modification of the microcin E492 C-terminus: linkage of ribosomal and nonribosomal peptides to form 'trojan horse' antibiotics. *Biochemistry* **47:** 9289–9299

Novoa MA, Diaz-Guerra L, San Millan JL, Moreno F (1986) Cloning and mapping of the genetic determinants for microcin C7 production and immunity. *J Bacteriol* **168:** 1384–1391

Otwinowski Z, Minor W (1997) Processing of X-ray diffraction data collected in oscillation mode. *Methods Enzymol* **276:** 307–326

Park JH, Dorrestein PC, Zhai H, Kinsland C, McLafferty FW, Begley TP (2003) Biosynthesis of the thiazole moiety of thiamin pyrophosphate (vitamin B1). *Biochemistry* **42:** 12430–12438

Pearce MJ, Mintseris J, Ferreyra J, Gygi SP, Darwin KH (2008) Ubiquitin-like protein involved in the proteasome pathway of Mycobacterium tuberculosis. *Science* **322:** 1104–1107

Pickart CM, Eddins MJ (2004) Ubiquitin: structures, functions, mechanisms. *Biochim Biophys Acta* **1695:** 55–72

Rajagopalan KV (1997) Biosynthesis and processing of the molybdenum cofactors. *Biochem Soc Trans* **25:** 757–761

Roush RF, Nolan EM, Lohr F, Walsh CT (2008) Maturation of an Escherichia coli ribosomal peptide antibiotic by ATP-consuming N-P bond formation in microcin C7. *J Am Chem Soc* **130:** 3603–3609

Severinov K, Semenova E, Kazakov A, Kazakov T, Gelfand MS (2007) Low-molecular-weight post-translationally modified microcins. *Mol Microbiol* **65:** 1380–1394

Shatsky M, Nussinov R, Wolfson HJ (2004) A method for simultaneous alignment of multiple protein structures. *Proteins* **56:** 143–156

Souphron J, Waddell MB, Paydar A, Tokgoz-Gromley Z, Roussel MF, Schulman BA (2008) Structural dissection of a gating mechanism preventing misactivation of ubiquitin by NEDD8's E1. *Biochemistry* **47:** 8961–8969

Terwilliger TC (2000) Maximum-likelihood density modification. *Crystallogr D Biol Crystallogr* **56:** 965–972

Terwilliger TC, Berendzen J (1999) Automated MAD and MIR structure solution. *Crystallogr D Biol Crystallogr* **55** (Part 4)**:** 849–861

Tokgoz Z, Bohnsack RN, Haas AL (2006) Pleiotropic effects of ATP.Mg2 + binding in the catalytic cycle of ubiquitin-activating enzyme. *J Biol Chem* **281:** 14729–14737

Walden H, Podgorski MS, Huang DT, Miller DW, Howard RJ, Minor Jr DL, Holton JM, Schulman BA (2003a) The structure of the APPBP1-UBA3-NEDD8-ATP complex reveals the basis for selective ubiquitin-like protein activation by an E1. *Mol Cell* **12:** 1427–1437

Walden H, Podgorski MS, Schulman BA (2003b) Insights into the ubiquitin transfer cascade from the structure of the activating enzyme for NEDD8. *Nature* **422:** 330–334

Walker JE, Saraste M, Runswick MJ, Gay NJ (1982) Distantly related sequences in the alpha- and beta-subunits of ATP synthase, myosin, kinases and other ATP-requiring enzymes and a common nucleotide binding fold. *EMBO J* **1:** 945–951

Xi J, Ge Y, Kinsland C, McLafferty FW, Begley TP (2001) Biosynthesis of the thiazole moiety of thiamin in Escherichia coli: identification of an acyldisulfide-linked protein—protein conjugate that is functionally analogous to the ubiquitin/E1 complex. *Proc Natl Acad Sci USA* **98:** 8513–8518

